

Controllable Preparation of a Three-Dimensional Porous Lead Dioxide Electrode with an Oxygen Bubble Template and Its Electrocatalytic Performance

Qi Hu, Qiang Yu*, Zhen Chen, Wei Zhu, Yuanyuan Liu, Zhaoyi Zheng, Lai Gui, Yuzhu Song

Faculty of Science, Kunming University of Science and Technology, Kunming 650093, China

*E-mail: yuqiang0015@163.com

Received: 3 August 2020 / Accepted: 10 November 2020 / Published: 30 November 2020

Three-dimensional porous PbO₂ (3D-PbO₂) electrode was prepared by anodic oxidation deposition method, using an oxygen bubble template. To prepare 3D-PbO₂ electrode controllably, the influence of current density, Pb²⁺ ion concentration, and pH value on the structure and performance of PbO₂ electrode was studied. The results show that the current density determined the appearance of oxygen bubbles. The nucleation and growth of the oxygen bubbles were controlled by Pb²⁺ concentration and the pH value, respectively. The effect of the process conditions on the performance of electrode materials was obtained by comparing the electrocatalytic activities of the electrodes. The morphology and phase composition of the different anode materials were analyzed, and electrocatalytic activities were investigated by cyclic voltammetry (CV) and electrochemical impedance spectroscopy (EIS). The CV curve shows that the total voltammetric charge (q_T^*) of the 3D-PbO₂ electrode was 70 times larger than that of the flat-PbO₂ electrode. In addition, during the evolution of oxygen, the 3D-PbO₂ electrode had a higher exchange current density (j^0), lower apparent activation energy (E_a) and lower charge transfer resistance (R_{ct}) than the flat-PbO₂ electrode.

Keywords: oxygen bubble template method; controllable preparation; lead dioxide; anode materials; electrocatalytic performance

1. INTRODUCTION

PbO₂-coated electrodes have a bright future owing to their good conductivity and catalytic activity, and many studies have shown that PbO₂ has excellent chemical reaction activity[1]. To improve the catalytic activity of PbO₂ electrode materials, doping or codeposition are primarily done to change the phase composition of the electrode and enhance the electrochemical active surface area (ECSA) of PbO₂ electrode material [2-4]. However, for the a traditional flat electrodes, only the electrode surface

can be infiltrated by the electrolyte, which limits the performance improvement of the electrode materials.

Porous materials have many features, such as large active surface areas, unique structures, and favorable interface reactions[5, 6]. By constructing porous electrode materials, changing electrode surface structure, increasing specific surface area and increasing active site number, the catalytic activity of electrode materials can be improved. Methods for preparing porous foamed metal materials typically involve electrodeposition based on different hard templates, such as alumina, silicon dioxide[7, 8] and polymer spheres[9, 10]. Chai et al.[11] prepared 3D-PbO₂ electrodes with a larger active surface area on a titanium substrate using polystyrene (PS) microspheres as a template, which enhanced the electrocatalytic activity of the PbO₂ electrode. Chahrour et al.[12] successfully prepared porous ZnO using an AAO template and investigated its structure and properties. However, the use of these templates inevitably involves the removal of template material through complicated processing steps after deposition, and the uniformity of the template is difficult to control.

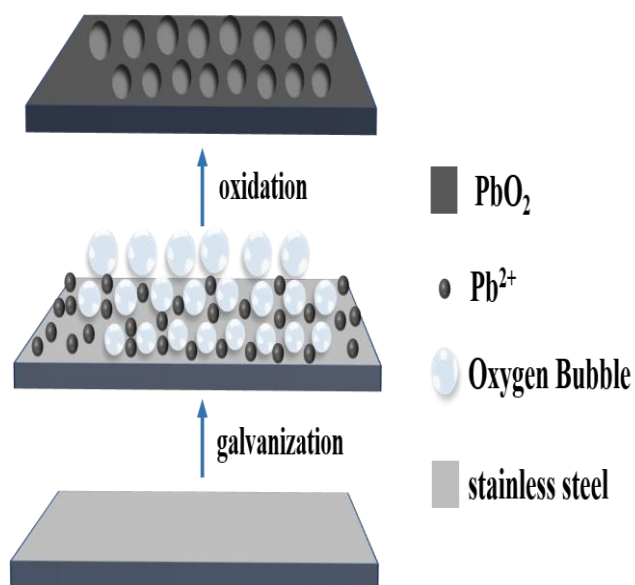


Figure 1. Schematic illustration of 3D-PbO₂ electrode was prepared based on oxygen bubble template method

In recent years, the bubble template method has attracted extensive research interest because of its advantages of simple process, controllability and low cost. The bubble template method usually takes hydrogen or oxygen bubble as template in the highly polarized conditions, the metal redox reaction takes place between pores, thus obtaining a porous structure[13-15]. The oxygen bubble template method[16-19] causes an oxygen evolution reaction on the anode surface through a high current during electrodeposition, and many oxygen bubbles take shape on the material surface. At the same time, the oxidation reaction occurs in the gap between the "template" of the bubbles. With time increasing, the oxygen bubbles separate from the substrate, and then porous electrode materials are obtained. Therefore,

the active surface area of porous electrodes is affected by pore size and pore density. However, few studies have reported the effects of electrodeposition conditions on porous structures.

A schematic illustration of the 3D-PbO₂ electrode was prepared based on oxygen bubble template method (Fig.1). To control the preparation of a 3D-PbO₂ electrode, the effects of the Pb²⁺ ion concentration, pH, and applied current density on the morphology and performance are studied. The surface morphology and composition of the electrode were investigated using scanning electron microscopy (SEM) and powder X-ray diffraction (XRD), the difference of activity between Flat and 3D electrode materials in Na₂SO₄ solution were also examined.

2. EXPERIMENTAL

2.1. Methods

Using oxygen bubbles as a template, 3D-PbO₂ electrodes were prepared via the anodic oxidation electrodeposition method. The anode was made of stainless steel sheet(10 mm×50 mm×1 mm), the cathode was made of stainless steel sheet(20 mm×50 mm×1 mm),. Those sheets were both polished with sandpaper, degreased, activated in hydrochloric acid solution, and washed in deionized water. Electrodeposition was carried out in lead nitrate plating solution containing 15 g·L⁻¹ Cu (NO₃)₂ and 27 g·L⁻¹ CH₃COONa·3H₂O, during electrodeposition, the temperature was maintained at 50 °C, and the plating time was 60 s. In separate experiments, the applied current density(0.5, 1.0, 1.5, 2.0, and 2.5 A·cm⁻²), the concentration of Pb²⁺ ion concentration(0.2, 0.3, 0.4, 0.5, and 0.6 mol·L⁻¹), and the pH value(2.0, 2.5, 3.0, 3.5, and 4.0) were studied. The flat-PbO₂ electrode material was prepared via anodic oxidation at a current density of 5 mA·cm⁻² for 30 min using a constant-current power supply at 50 °C. The aqueous solution was made up of 190 g·L⁻¹ Pb (NO₃)₂, 0.5 g·L⁻¹ NaF, and 15 g·L⁻¹ Cu (NO₃)₂, and the pH value was 3.

2.2. Materials characterizations

The surface morphology of the PbO₂ electrodes was obtained by SEM. The pore size and number in the electrode were calculated by Image-Pro Plus. The phase composition was determined by XRD. All electrochemical measurements were conducted on a CHI660D electrochemical workstation with a standard three-electrode cell in 0.5 mol·L⁻¹ Na₂SO₄ solution at 25 °C. The PbO₂ electrode (10 mm×10 mm) was used as the working electrode, a saturated calomel electrode (SCE) served as the reference electrode, and the counter electrode was a Pt sheet. LSV at a scan rate of 5 mV·s⁻¹ from 0.5 to 1.8V vs. SCE. LSVs were collected to obtain the exchange current density, The Tafel region was selected for linear fitting. Additionally, the linear region was employed to obtain the potential (E) of oxygen evolution[20]. LSV was measured at 25-45 °C to acquire the E_a, the E_a can be obtained through the following Arrhenius law. The ECSA of the electrode materials was calculated by CV, the test range from 0.8-1.0V, and the scanning rate was 5,10, 20, 40, 60, 80, 100, and 120 mV·s⁻¹. The charge transfer resistance was measured via EIS, the initial potential was chosen to be in the stable oxygen evolution reaction potential region (1.65V), and the frequency ranged from 10⁵ Hz to 0.05 Hz.

3. RESULTS AND DISCUSSION

3.1 Effect of the current density

The dependence of the film morphology on the current densities are presented in Fig.2. Average diameter and hole number were determined by Image Pro Plus, to analyze the influence of the current density on the pore size distribution of the 3D-PbO₂ (Fig.3). It can be seen from Fig.2 (a) that when the current density was 2.0 A·cm⁻², the fine and dense grains are uniformly distributed on the stainless steel substrates. When the current density was increased to 1.0 A·cm⁻²(Fig.2 (b)), some pores began to form, but were not uniformly distributed on the substrate surface. This phenomenon can be attributed to slow oxygen evolution and insufficient amount of bubbles owing to the low current density. As the current density increased, oxygen bubbles gradually and uniformly formed on the material base. In addition, the nucleation and growth of the PbO₂ crystal tended to be complete, the surface morphology changed from a flat structure to a porous structure. A film with uniformly distributed macro-pores was obtained when the current density was increased to 1.5 A·cm⁻²(Fig.2 (c)), the number of pores was 1973/mm², the average pore size was approximately 8.3 μm. When the current density was 2.0 A·cm⁻², the number of pores reached 2092/mm², mean pore size was 7.9 μm, the surface pore diameter decreased and the number of pores increased (Fig.2 (d)). The increase of current density promoted the increase of oxygen precipitation and PbO₂ deposition rate. This is in agreement with the results that a higher gas evolution rate leads to the formation of smaller gas bubbles and eventually to the formation of pores with a smaller diameter[21]. When the current density was 1.5-2.5 A·cm⁻², the pore size of the surface decreased at first and then increased (Fig.2 (c₃-e_{3-2, the number of pores decreased to 1613/mm², and the mean pore size increased by 8.5 μm. The oxygen evolution rate increased as the applied current density increased, causing strong electrolyte turbulence around the oxygen bubbles, which increased the driving force for the oxygen bubbles to move away from the electrode surface and decreased the oxygen bubble diameter. when the current density was 2.5 A·cm⁻², the electrode surface absorbs a large number of oxygen bubbles, on the one hand, increased the possibility of oxygen bubbles merging, slightly increases the bubble diameter; on the other hand, limited the load of surface-active material, resulting in the decreased electrocatalytic performance.}

Fig. 4 shows the LSVs of 3D-PbO₂ electrodes prepared under different applied current densities. It can be seen that the LSV curves have an oxidation peak around 1.3V, which is due to the incomplete oxidation of PbO in the preparation process under the condition of high current density, which reflects the process of further oxidation of PbO to PbO₂ during the testing process[22], the current density increases sharply due to oxygen evolution reaction after 1.5V. Therefore, the electrocatalytic activity of the electrode was characterized by exchange current density and oxygen evolution potential, the kinetic parameters of oxygen evolution can be obtained by selecting the stable oxygen evolution zone for Tafel fitting (see Table 1). The electrode reaction was a heterogeneous catalytic reaction that occurred mainly at the electrode/solution interface, and j^0 is significant for the study of the electrocatalytic activity. A comparison of the exchange current density indicates the absolute velocity of the reaction of the electrode and the electrocatalytic activity of the electrode materials[23]. The larger j^0 is, the higher absolute reaction rate, and the easier electrode reaction. It can be seen that the oxygen evolution potential

decreased first and then increased, meanwhile j^0 increased first and then decreased. When the current density was $2.0 \text{ A}\cdot\text{cm}^{-2}$, the minimum oxygen evolution potential was 1.459 V, and the maximum exchange current density was $8.209 \times 10^{-7} \text{ A}\cdot\text{cm}^{-2}$, which indicates intense electrocatalytic activity for oxygen evolution. During the preparation process, when the current density is small, the precipitation rate of oxygen bubbles is slow, the deposition of the coating is dominated by grain growth, and the coating is smooth and compact. With the increase of current density, the three-dimensional porous structure tends to be complete, which shortened the ion exchange path in the electrolyte. Additionally, the increased of current density result in the refinement of PbO_2 grain, the increase of reaction space, and the enhancement of the electrocatalytic activity of electrode materials.

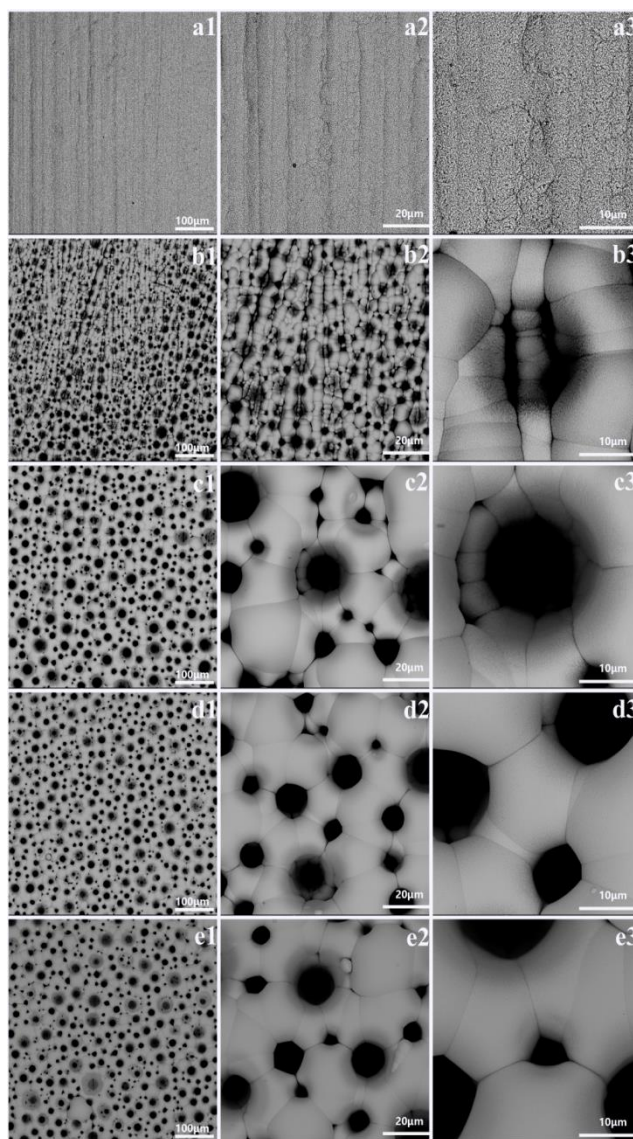


Figure 2. SEM micrographs showing different morphologies evolved due to variation of current densities at different magnifications $0.5 \text{ A}\cdot\text{cm}^{-2}$ (a₁-a₃), $1.0 \text{ A}\cdot\text{cm}^{-2}$ (b₁-b₃), $1.5 \text{ A}\cdot\text{cm}^{-2}$ (c₁-c₃), $2.0 \text{ A}\cdot\text{cm}^{-2}$ (d₁-d₃) and (e₁-e₃) $2.5 \text{ A}\cdot\text{cm}^{-2}$. 1, 2, and 3 magnifications of 500, 3000, and 8000 \times , respectively.

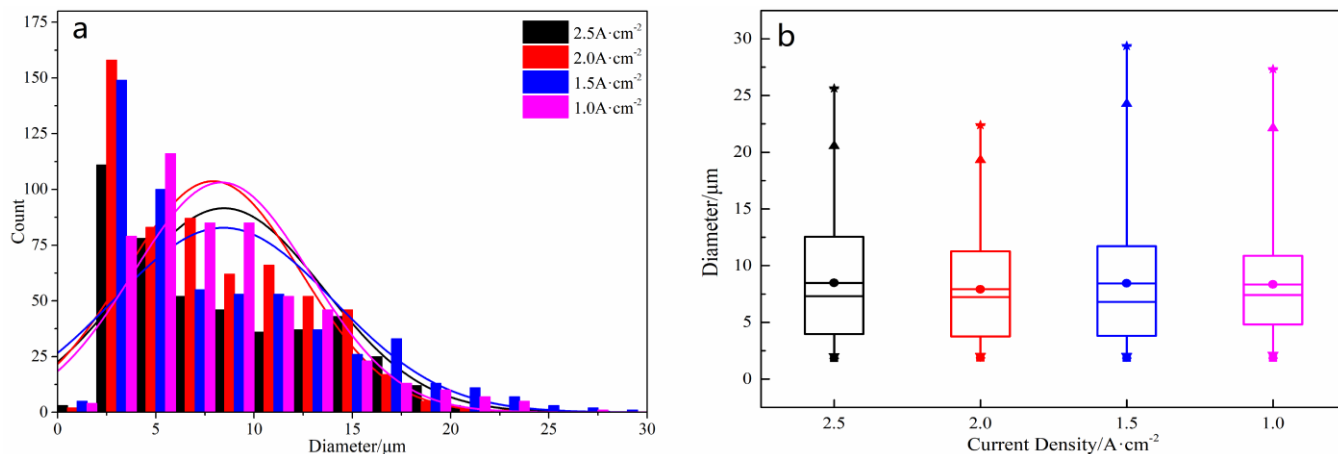


Figure 3. Statistical map of the pore size distribution of the 3D-PbO₂ electrode prepared at different current densities: histogram of pore size frequency distribution (a) and pore size box diagram (b).

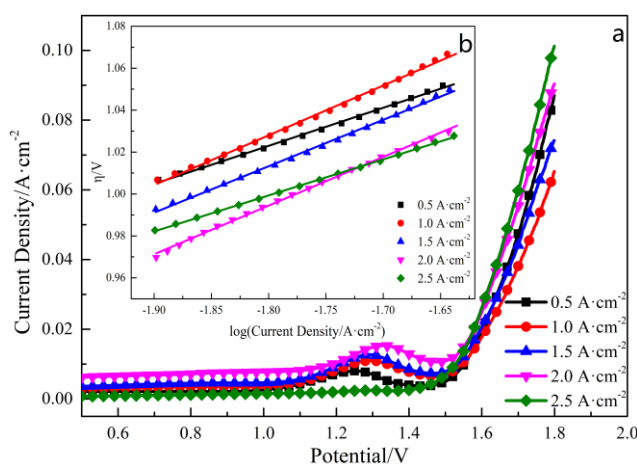


Figure 4. Linear sweep voltammograms (a) and linear fitting curves (b) of 3D-PbO₂ electrodes prepared under different current densities

Table 1. OER kinetic parameters of 3D-PbO₂ electrodes prepared at different current densities

Current Density/ A·cm ⁻²	a/ V	b/V·dec ⁻¹	j ⁰ / A·cm ⁻²	E/ V
0.5	1.350	0.181	3.642×10 ⁻⁸	1.511
1.0	1.455	0.220	2.426×10 ⁻⁷	1.494
1.5	1.412	0.221	4.189×10 ⁻⁷	1.485
2.0	1.412	0.232	8.209×10 ⁻⁷	1.459
2.5	1.308	0.172	2.404×10 ⁻⁸	1.491

When current density was 2.0 A·cm⁻², the pore size distribution of the oxygen bubbles was relatively concentrated, and the electrode surface showed a uniform porous structure with high electrocatalytic activity. Therefore, 2.0 A·cm⁻² was the best current density herein for the 3D-PbO₂ electrode.

3.2 Effect of the Pb^{2+} concentration

The SEM images presented in Fig.5 shows the effect of the Pb^{2+} concentration on the morphology of the PbO_2 film. Fig. 6a is a histogram of the distribution of the pore size frequency at different Pb^{2+} concentrations, and Fig.6b is a box diagram of the corresponding pore sizes.

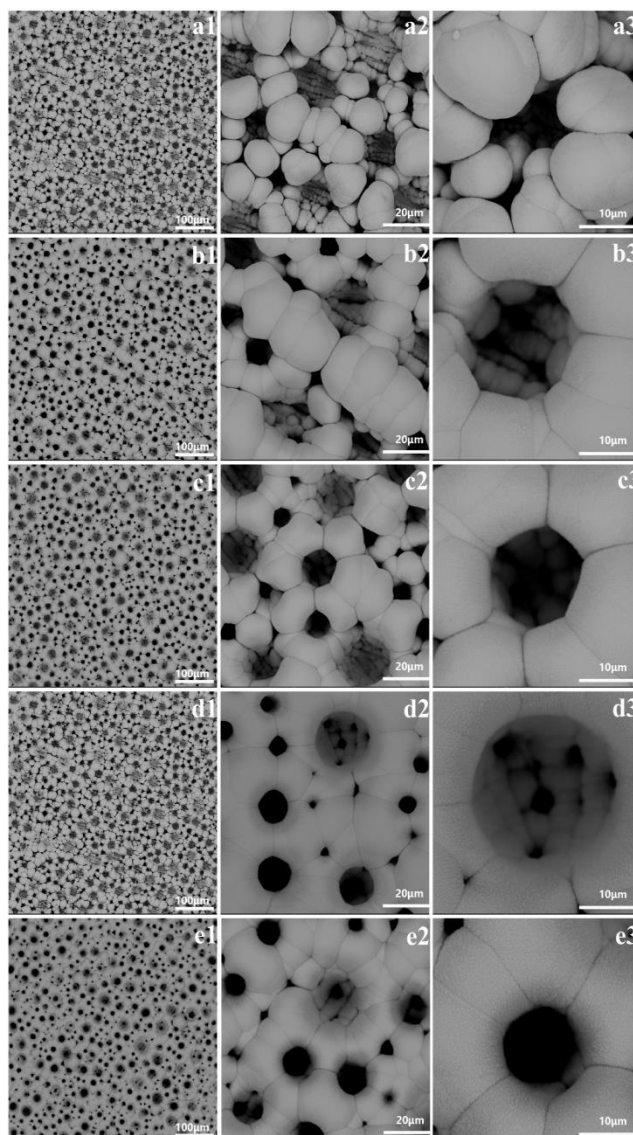


Figure 5. SEM micrographs showing different morphologies evolved due to variation of Pb^{2+} concentrations at different magnifications. $0.2 \text{ mol}\cdot\text{L}^{-1}$ (a1-a3), $0.3 \text{ mol}\cdot\text{L}^{-1}$ (b1-b3), $0.4 \text{ mol}\cdot\text{L}^{-1}$ (c1-c3), $0.5 \text{ mol}\cdot\text{L}^{-1}$ (d1-d3) and $0.6 \text{ mol}\cdot\text{L}^{-1}$ (e1-e3). 1, 2, and 3 magnifications of 500, 3000, and 8000 \times , respectively.

All of the deposits have a porous structure, but the morphologies are unique in each case (Fig.5 (a-e)). As the Pb^{2+} concentration increased, the space between the PbO_2 grains decreased, the electrode surface became smoother and more compact, the pore diameter decreased gradually, and the pore walls became thick (Fig.5 (a2-e2)). The porous structure was caused by the competition between the PbO_2 deposition and the oxygen evolution reaction. The increase in the Pb^{2+} concentration led to PbO_2

deposition is dominant, the wall of the films thickened with increasing Pb^{2+} concentration. When the Pb^{2+} concentration was $0.2 \text{ mol}\cdot\text{L}^{-1}$, some pores began to form, but were not complete (Fig.5 (a)). When the concentration of Pb^{2+} was low, the Pb^{2+} consumed on the electrode surface cannot be replenished in time to form the pore wall structure. It should be noted, that distribution of the particles is non-uniform, which is a result of non-uniform distribution of oxygen bubbles on the surface. When the Pb^{2+} concentration was increased to $0.4 \text{ mol}\cdot\text{L}^{-1}$, the pore diameter of the surface decreased slightly, the pore wall thickened, and the three-dimensional structure became complete. The number of pores was $2499/\text{mm}^2$, and the pore size was $8.14 \mu\text{m}$. With increasing Pb^{2+} concentration, the concentration polarization became weaker, which promoted the deposition of the PbO_2 nuclei and the oxygen evolution equilibrium. Under the condition of a constant current, the concentration of Pb^{2+} increased, oxygen evolution is reduced, the surface oxygen bubbles from the electrode materials decreased. the number of pores decreased to $1980/\text{mm}^2$ at $0.6 \text{ mol}\cdot\text{L}^{-1}$, the size of pore was $6.5 \mu\text{m}$.

Fig. 7 shows the LSV of 3D- PbO_2 electrodes prepared at different Pb^{2+} concentrations. Table 2 shows the corresponding kinetic parameters of oxygen evolution. It can be seen that with an increase in the Pb^{2+} concentration, the oxygen evolution potential of the electrode material decreased at first and then increased, and j^0 increased at first and then decreased. With increasing Pb^{2+} concentration, the electrode surface formed a complete and uniform three-dimensional porous structure, which increased the real active surface area of the materials. The porous structure enabled the electrolyte solution to enter the active layer, expanding the reaction space. Therefore, the electrode can fully contact with electrolyte, and promote electrocatalytic reaction. The results show that the minimum oxygen evolution potential was 1.502 V , and the maximum j^0 was $7.987 \times 10^{-6} \text{ A}\cdot\text{cm}^{-2}$ at $0.4 \text{ mol}\cdot\text{L}^{-1}$, which indicated a relatively stable electrocatalytic activity.

The results show that when the concentration of Pb^{2+} was $0.4 \text{ mol}\cdot\text{L}^{-1}$, Electrodes had uniform porous structure and excellent electrocatalytic activity. Therefore, the optimal concentration of Pb^{2+} was $0.4 \text{ mol}\cdot\text{L}^{-1}$ herein.

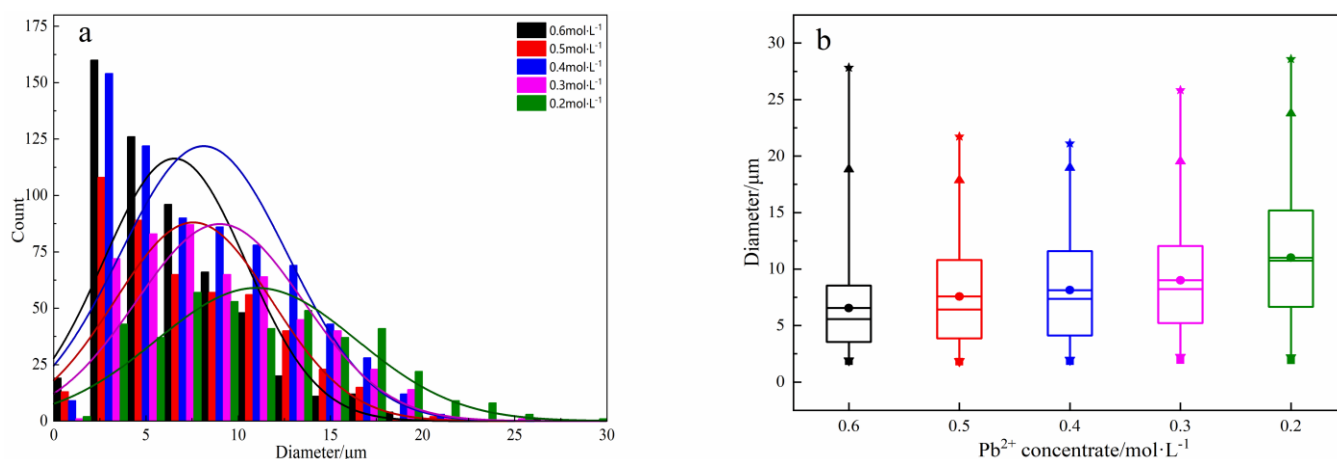


Figure 6. Statistical map of the pore size distribution of the 3D- PbO_2 electrode prepared at different Pb^{2+} concentrations: histogram of pore size frequency distribution (a) and pore size box diagram (b).

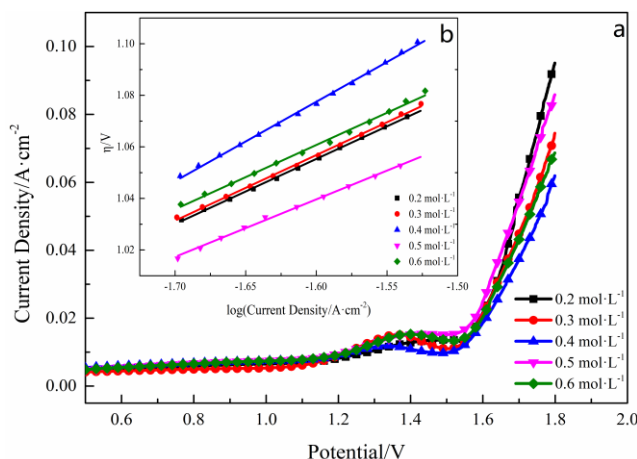


Figure 7. Linear sweep voltammograms (a) and linear fitting curves (b) of 3D-PbO₂ electrodes prepared at different Pb²⁺ concentrations

Table 2. OER kinetic parameters of 3D-PbO₂ electrodes prepared at different Pb²⁺ concentrations

Pb ²⁺ concentration/ mol·L ⁻¹	a/ V	b/V·dec ⁻¹	j ⁰ / A·cm ⁻²	E/ V
0.2	1.460	0.253	1.672×10 ⁻⁶	1.505
0.3	1.464	0.254	1.761×10 ⁻⁶	1.504
0.4	1.570	0.308	7.987×10 ⁻⁶	1.502
0.5	1.397	0.223	5.508×10 ⁻⁷	1.511
0.6	1.460	0.226	3.347×10 ⁻⁷	1.512

3.3 The effect of the pH

To reveal the influence of acidity on the formation of porous PbO₂, the SEM images of 3D-PbO₂ electrodes formed under different pH values were investigated(Fig.8). Fig. 9a is a histogram of the pore size frequency distribution, and Fig. 9b is a box diagram of the pore sizes. All of the deposits have porous structures and similar morphologies at different pH conditions (Fig.8 (a₂-e₂)). when the pH value was 2.0 (Fig.8 (a₂)), the pore diameter difference of the active layer was large, and the pore wall was thick, the number of surface pores reached 2048/mm², the average pore size was 7.6 μm. As the concentration of OH⁻ increased, the oxygen bubbles precipitated quickly, which led to an increase in pores density and improved the internal connectivity of the electrode. The pH value of the solution was increased, mass of oxygen bubbles adsorbed on the electrode, then they are aggregated and escaped, thus resulting in increased pore diameter and decreased pores density (Fig.8 (c₂-e₂)). when the pH value was 3.0, a large number of oxygen bubbles appeared, the pore diameter difference decreased, the number of surface pores reached 2143/mm², the range of the largest and smallest pore size was reduced to 17.6μm, the mean size

was $7.8\mu\text{m}$, and the pore wall became thin (Fig.8 (c₃)). when the pH value was 4.0, the number of pores on the surface decreased to $2007/\text{mm}^2$, the average size was $10.2\mu\text{m}$. The result shows that pH value had little effect on the number of pores, but the pore size and uniformity could be controlled.

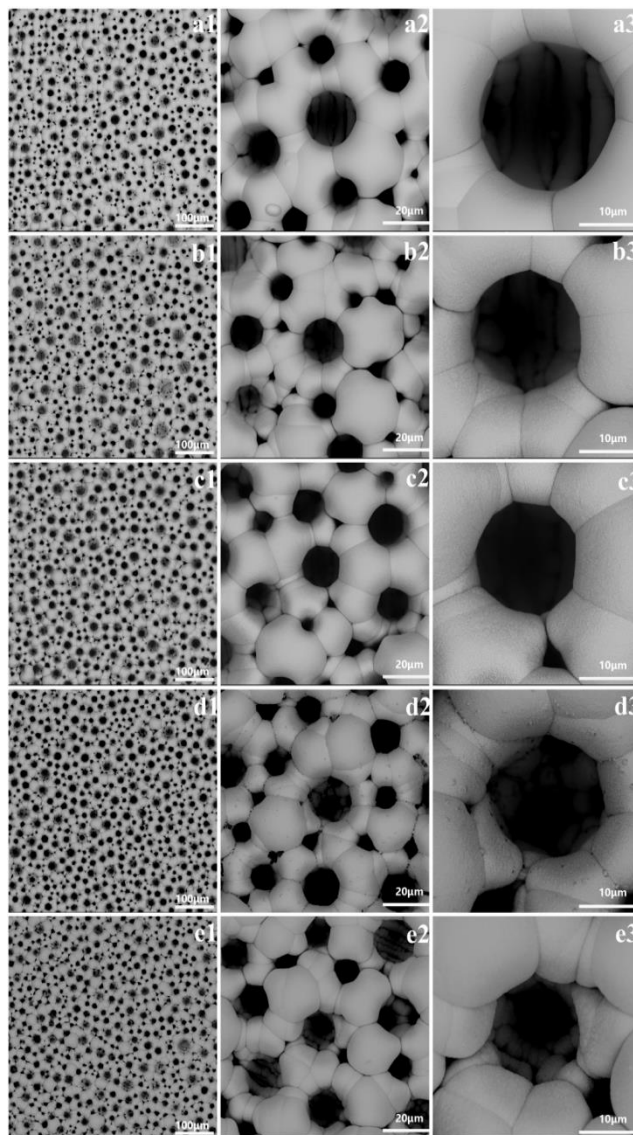


Figure 8. SEM micrographs showing different morphologies evolved due to variation of pH values at different magnifications. 2.0 (a₁-a₃), 2.5 (b₁-b₃), 3.0 (c₁-c₃), 3.5 (d₁-d₃) and 4.0 (e₁-e₃). 1, 2, and 3 magnifications of 500, 3000, and 8000 \times , respectively.

The LSV of the 3D-PbO₂ electrodes prepared at different pH values are shown in Fig.10. The corresponding kinetic parameters for the oxygen evolution are listed in Table 3, where it can be seen that the oxygen evolution potential of the electrode material decreased first and then increased, and j^0 increased first and then decreased. The minimum oxygen evolution potential was 1.481 at pH 3.0, and the maximum j^0 was $6.378 \times 10^{-6} \text{ A}\cdot\text{cm}^{-2}$ at pH 3.0. The current density increased quickly when the electrode material prepared at pH 3.0 reached the oxygen evolution potential. The increased slope of the curve indicates that the electrode reaction took place very quickly on the material base during

electrocatalysis when there was a high current density at the same potential. With increasing pH, the electrode surface became denser and more uniform, the active surface area of the electrode material was increased by the grains on the pore wall, the electrocatalytic activity of the electrode was enhanced. Therefore, the optimum 3D-PbO₂ electrode material was obtained by setting the optimum pH value of the bath solution at 3.0.

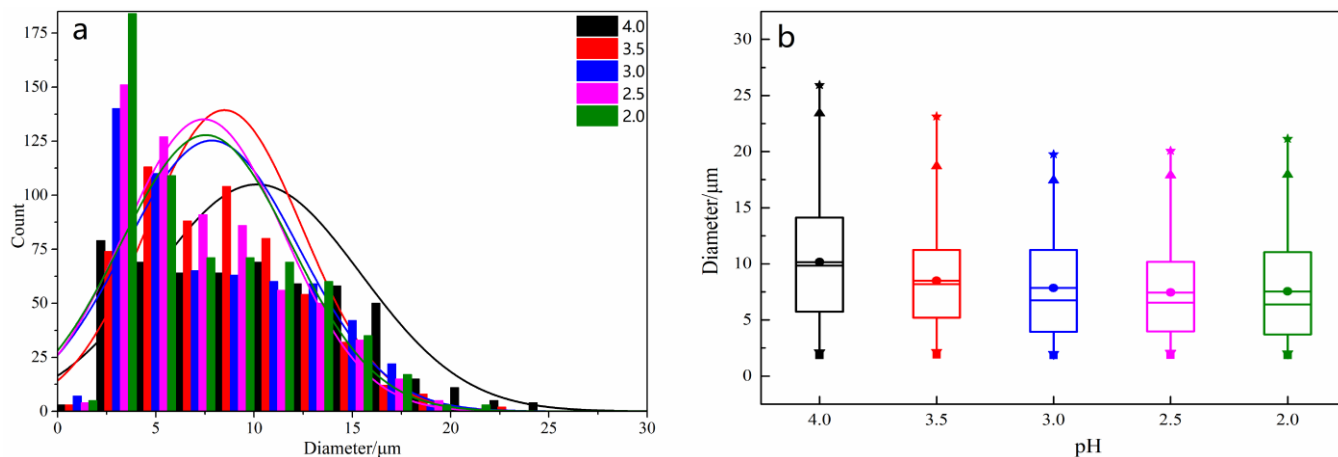


Figure 9. Statistical map of the pore size distribution of the 3D-PbO₂ electrode prepared at different pH values: histogram of pore size frequency distribution (a) and pore size box diagram (b).

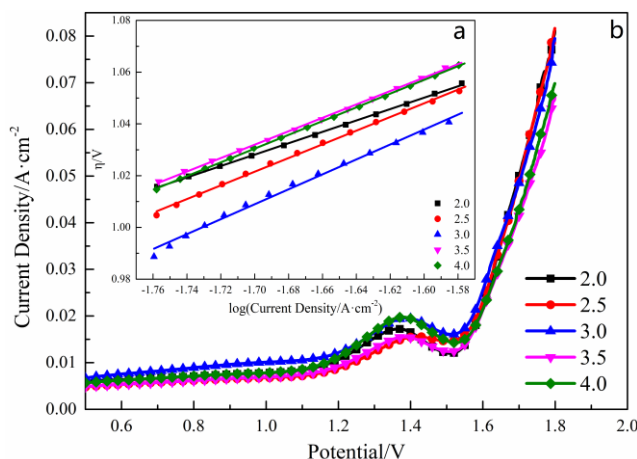


Figure 10. Linear sweep voltammograms (a) and linear fitting curves (b) of 3D-PbO₂ electrodes prepared at different pH values

Table 3. OER kinetic parameters of 3D-PbO₂ electrodes prepared at different pH values

pH	a/ V	b/V·dec ⁻¹	j ⁰ / A·cm ⁻²	E/ V
2.0	1.402	0.220	4.246×10 ⁻⁷	1.508
2.5	1.471	0.264	2.720×10 ⁻⁶	1.495
3.0	1.500	0.289	6.378×10 ⁻⁶	1.481
3.5	1.473	0.266	2.863×10 ⁻⁶	1.492
4.0	1.482	0.259	1.914×10 ⁻⁶	1.495

3.4 Comparison of the electrocatalytic activity of the different electrodes

3.4.1 Microscopic morphology

SEM images of the flat-PbO₂ electrode and the 3D-PbO₂ electrode were acquired and shown in Fig. 11. In Fig. 11a, the flat-PbO₂ crystal shows a rutile structure, which is a typical structure of PbO₂. As shown in Fig.11b, Compared with the flat-PbO₂ electrode, the 3D-PbO₂ electrode had a three-dimensional porous structure with a pore size of approximately 10 μm, and the pores were surrounded by a large number of refined PbO₂ grains. The 3D-PbO₂ electrode had an elevated probability of lattice distortion at the interface and formed abundant surface defect sites. These defect sites can increase the number of active sites on the electrode. The interconnecting cavities increased the ion diffusion in the electrolyte and the permeation flux. The cavities allowed the electrolyte to contact the active center in the active layer and provided a large active surface area for electrocatalysis, thus enhancing the electrochemical activity of the electrode material.

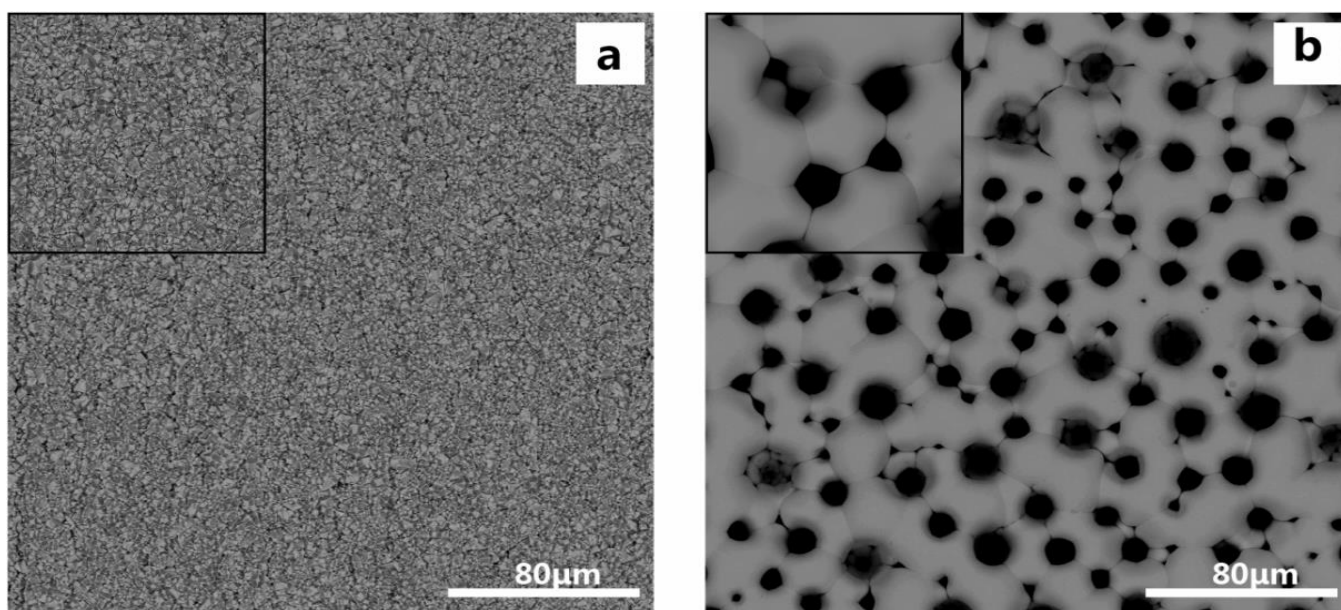


Figure 11. SEM images of flat-PbO₂ electrode (a) and 3D-PbO₂ electrode (b) (1000×)

3.4.2 Phase composition

The two electrode materials had obvious diffraction peaks at the positions of 25.4°, 31.9°, 36.2°, 49.1°, 62.5° and 74.4° (Fig.12). Both of the materials contained β-PbO₂ (PDF # 41-1492). Upon comparing the XRD patterns of the two kinds of electrodes, it can be seen that the intensity of diffraction peaks of the 3D-PbO₂ electrode materials increased obviously at 49.1° but decreased obviously at 25.4°, 31.9° and 62.5°. The three-dimensional porous structure of the PbO₂ electrode influenced the growth orientation of the crystals. All peaks are very wide or have poor resolution because the porous PbO₂ consists of very small microcrystals, this result was also confirmed in the study of Nicola[24].

According to the Debye-Scherrer formula, the width of a diffraction peak is inversely proportional to the grain size; that is, the wider the diffraction peak is, the smaller the grain size[25, 26]. The results show that the average grain size of the 3D-PbO₂ was smaller than that of the flat-PbO₂, the average grain sizes of the flat-PbO₂ and 3D-PbO₂ were 35 nm and 6 nm, respectively. The reason is that under the condition of a high current density, the nucleation of the PbO₂ increased, which refined the grains, formed a uniform particle coating.

The reason is that under the condition of a high current density, the nucleation of the PbO₂ increased, which refined the grains, formed a uniform particle coating.

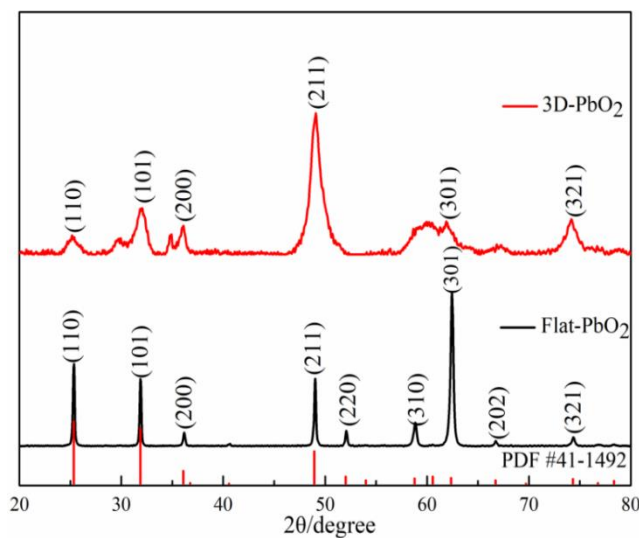


Figure 12. XRD of flat-PbO₂ electrode and 3D-PbO₂ electrode

3.4.3 Linear sweep voltammograms

The electrocatalytic performance of the electrode materials was characterized by the oxygen evolution potential. The lower the oxygen evolution potential was, the easier the oxygen evolution reaction, and the better the electrocatalytic performance of the corresponding electrode. Fig. 13 shows the LSV of the two electrode materials, the oxygen evolution potential of the 3D-PbO₂ electrode was 1.455 V, which is lower than the 1.629 V for the flat-PbO₂ electrode. Wang et al.[27] prepared a series of PbO₂ anode materials by adding different surfactants. The minimum oxygen evolution potential of different PbO₂ electrodes is 1.57V, while in this study, the oxygen evolution potential of 3D-PbO₂ anode materials is only 1.455, which shows better electrocatalytic performance than the smaller oxygen evolution potential.

Table 4 shows the oxygen evolution kinetic parameters of the two electrodes. The j^0 of the 3D-PbO₂ electrode was $1.105 \times 10^{-6} \text{ A} \cdot \text{cm}^{-2}$, which is higher than the flat-PbO₂ electrode value of $6.747 \times 10^{-7} \text{ A} \cdot \text{cm}^{-2}$. Fig. 13 shows that the 3D-PbO₂ electrode had a higher current density at a lower initial potential. Therefore, the 3D-PbO₂ electrode had better electrocatalytic activity than the flat-PbO₂ electrode. The 3D-PbO₂ electrode prepared by oxygen bubble template method has refined grain,

increased the electrochemical active surface area of the electrode material, and enhanced its electrocatalytic activity.

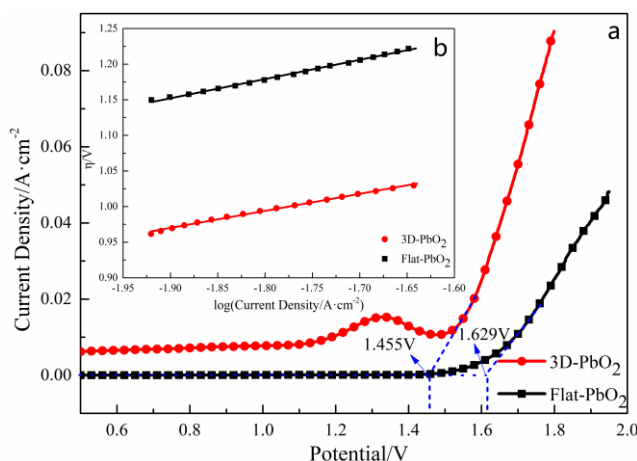


Figure 13. Linear sweep voltammograms (a) and linear fitting curves (b) of the flat-PbO₂ electrode and 3D-PbO₂ electrode

Table 4. Oxygen evolution kinetic parameters of the flat-PbO₂ electrode and 3D-PbO₂ electrode

Electrode	a/ V	b/V·dec ⁻¹	j ⁰ / A·cm ⁻²	E/ V
3D-PbO ₂ Electrode	1.424	0.239	1.105×10 ⁻⁶	1.455
flat-PbO ₂ Electrode	1.665	0.270	6.747×10 ⁻⁷	1.629

3.4.4 Electrochemical active surface area

The electrochemical activity of PbO₂ is related to its real surface area and the number of active sites in contact with the electrolyte. At the same time, the volt-ampere charge (q*) is related to the real active surface area and is affected by the active sites. The value of q* is widely regarded as a measure of the electrochemical activity of a site; a larger q* indicates a higher electrochemical activity[28, 29]. To study the electrochemical activity of the PbO₂ electrode, the active surface area and the effective active sites of the different electrode materials were evaluated by the volt-ampere charge quantity q*.

During the electrochemical reaction process, the total number of electrochemical sites is the sum of the surface and bulk electrochemical reaction sites, and the reaction shows the total volt-ampere charge q_T^{*}, external volt-ampere charge q_o^{*} and internal volt-ampere charge q_i^{*}.

The value of q_T^{*} can be obtained by the reciprocal volt-ampere charge of the electrode at different sweep speeds and the square root of sweep speeds by formula 4[30] :

$$1/q^* = 1/q_T^* + kv^{1/2} \tag{3}$$

The q_o^* quantity of the electrode material represents a charge related to the external active surface directly exposed to the electrolyte, which is obtained by Formula 5[31]:

$$q^* = q_o^* + k'v^{-1/2} \tag{4}$$

The corresponding q_i^* is obtained from Formula 6, which indicates the charges related to the internal active surface hidden in the loose grain boundaries, pores and cracks[32]:

$$q_T^* = q_i^* + q_o^* \tag{5}$$

Fig. 14 shows the CV curve and the corresponding curve of the flat-PbO₂ electrode and 3D-PbO₂ electrode in a 0.5 mol·L⁻¹ Na₂SO₄ solution. Table 5 shows that the q_T^* was $4.87 \times 10^{-2} \text{ C} \cdot \text{cm}^{-2}$, the q_o^* was $5.89 \times 10^{-3} \text{ C} \cdot \text{cm}^{-2}$, and the q_i^* was $4.28 \times 10^{-2} \text{ C} \cdot \text{cm}^{-2}$ for the 3D-PbO₂ electrode.

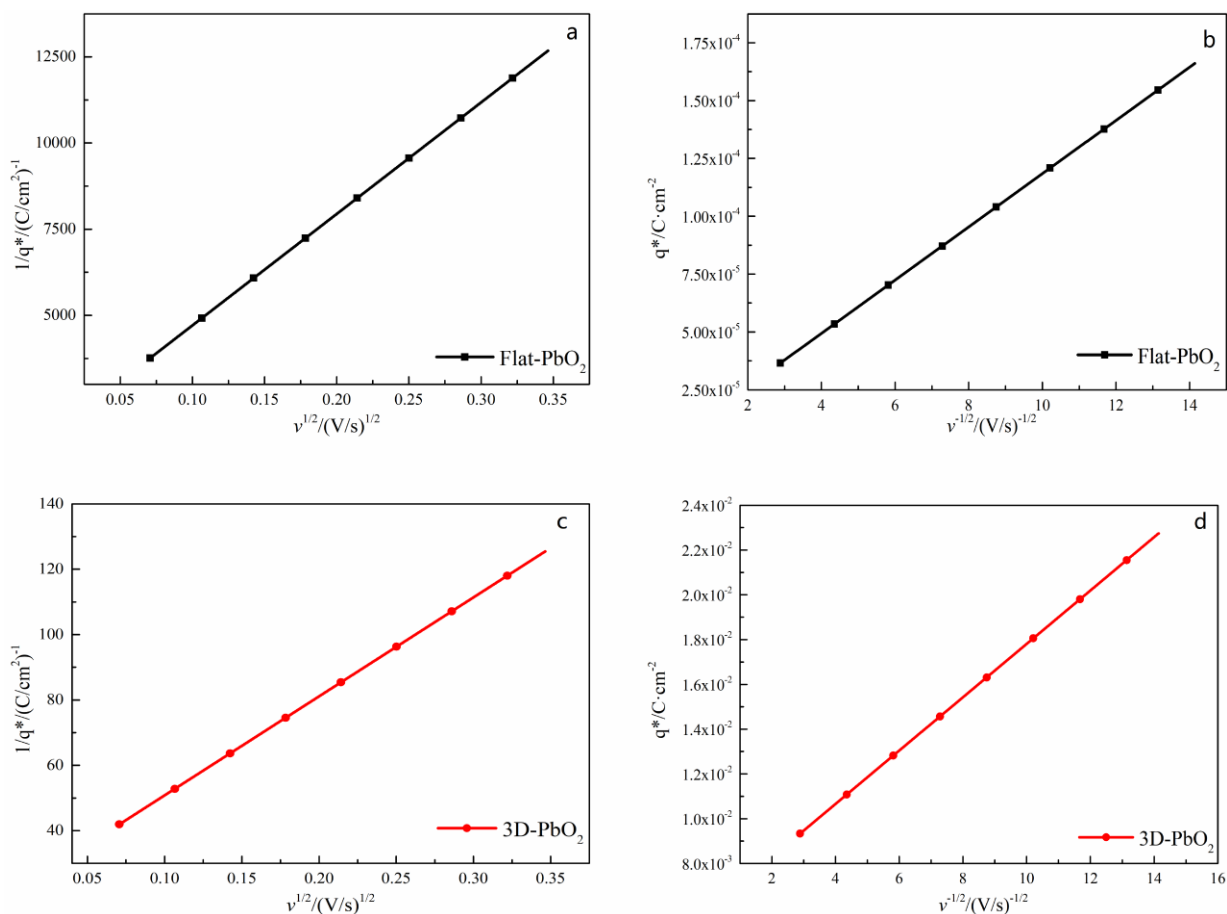


Figure 14. $1/q^* \cdot v^{1/2}$ curves for the flat-PbO₂ (a) and 3D-PbO₂ (c) electrodes; $q^* \cdot v^{-1/2}$ curves for the flat-PbO₂ (b) and 3D-PbO₂ (d) electrodes

The volt-ampere charges of the flat-PbO₂ electrode were $6.80 \times 10^{-4} \text{ C} \cdot \text{cm}^{-2}$, $6.75 \times 10^{-6} \text{ C} \cdot \text{cm}^{-2}$, and $6.73 \times 10^{-4} \text{ C} \cdot \text{cm}^{-2}$. The data show that the 3D-PbO₂ electrode had a larger q_T^* than the flat-PbO₂ electrode, which indicates that the 3D-PbO₂ electrode had better electrocatalytic activity. Wang et al. [27] prepared and optimized a series of PbO₂ electrodes by adding different surfactants, the maximum total volt-ampere charge of 3D-PbO₂ is $3.69 \times 10^{-2} \text{ C} \cdot \text{cm}^{-2}$. In this study, the total volt-ampere charge of 3D-PbO₂

electrode is $4.87 \times 10^{-2} \text{ C}\cdot\text{cm}^{-2}$, Compared with it, 3D-PbO₂ electrode has larger electrochemical active surface area, which is beneficial to the improvement of electrocatalytic activity. Zhou et al.[33] adopted PS microspheres as a templates and added TiO₂ to prepare TiO₂/SnO₂-Sb/3D porous PbO₂ electrode, electrodes with internal and external voltammetric charges of 1.45×10^{-2} and $2.20 \times 10^{-2} \text{ C}\cdot\text{cm}^{-2}$. Compared with this electrode, the 3D-PbO₂ electrode prepared in this study has larger internal and external volt-ampere charges and provides more reaction sites in the electrocatalytic reaction to improve the catalytic performance.

The main reason for the large increase in the q_o^* of the 3D-PbO₂ electrode is that the elevated current density led to a fast nucleation rate of the PbO₂ crystals, a fine-grained coating, and an increase in the active surface area between the electrode surface and the electrolyte. In addition, because the porous structure of the 3D-PbO₂ electrode increased the electrolyte permeability and promoted the ion adsorption/exchange on the electrode material, the q_i^* of the 3D-PbO₂ electrode was larger than that of the flat-PbO₂ electrode. The porous structure also increased the internal active surface area of the electrode material, provide more active sites for the reaction, promoting further promotion of the electrocatalytic activity of the electrode material[34].

Table 5. Voltammetric charge of the flat-PbO₂ electrode and 3D-PbO₂ electrode

Electrode	q_T^* (C·cm ⁻²)	q_o^* (C·cm ⁻²)	q_i^* (C·cm ⁻²)
3D-PbO ₂ Electrode	4.87×10^{-2}	5.89×10^{-3}	4.28×10^{-2}
flat-PbO ₂ Electrode	6.80×10^{-4}	6.75×10^{-6}	6.73×10^{-4}

3.4.5 Apparent activation energy

The E_a can be used to characterize the catalytic activity of the electrode, that is, the degree of difficulty of the electrode reaction. The greater number of active sites on the surface of the electrode material is, the smaller the E_a required for the reaction, the better the electrocatalytic activity of the electrode reaction, and the more likely the electrode reaction is to occur[35].

When the electrode process reaches the steady state, the non-faradaic charging process is essentially stable, and the external current is completely consumed by the electrode reaction. The faradaic current (j) is proportional to the electrode reaction rate, and the reaction rate is closely related to the reaction rate constant[36]. The polarization curves and linear fitting curves for the flat-PbO₂ and 3D-PbO₂ electrodes from 25 °C to 45 °C are shown in Figs. 15a and 15b, respectively. The E_a of the two electrode materials was obtained by fitting the slope of the curve, and the activation energy data are shown in Table 6. It can be seen that the E_a of 3D-PbO₂ electrode was 24.92 kJ·mol⁻¹, which is lower than that of the flat-PbO₂ electrode (30.53 kJ·mol⁻¹), this indicates that 3D-PbO₂ has a small energy barrier to cross during electrocatalysis, which promotes the reaction.

The microstructure and properties of the PbO₂ electrode materials were not uniform, only unique sites on their surfaces can adsorb and activate reactant molecules and thus play a catalytic role. These sites are called surface active sites or active centers. Therefore, increasing the active surface area can increase the density of the active sites on the unit surface and enhance the catalytic activity effectively. Because of the three-dimensional porous structure of the electrode, the number of active sites on the surface of the electrode increased, and the apparent activation energy of the oxygen evolution reaction decreased.

In summary, compared to the characteristics of the flat-PbO₂ electrode, the 3D-PbO₂ electrode had a larger active surface area, more active centers and a lower apparent activation energy for the oxygen evolution reaction because of its unique three-dimensional porous structure.

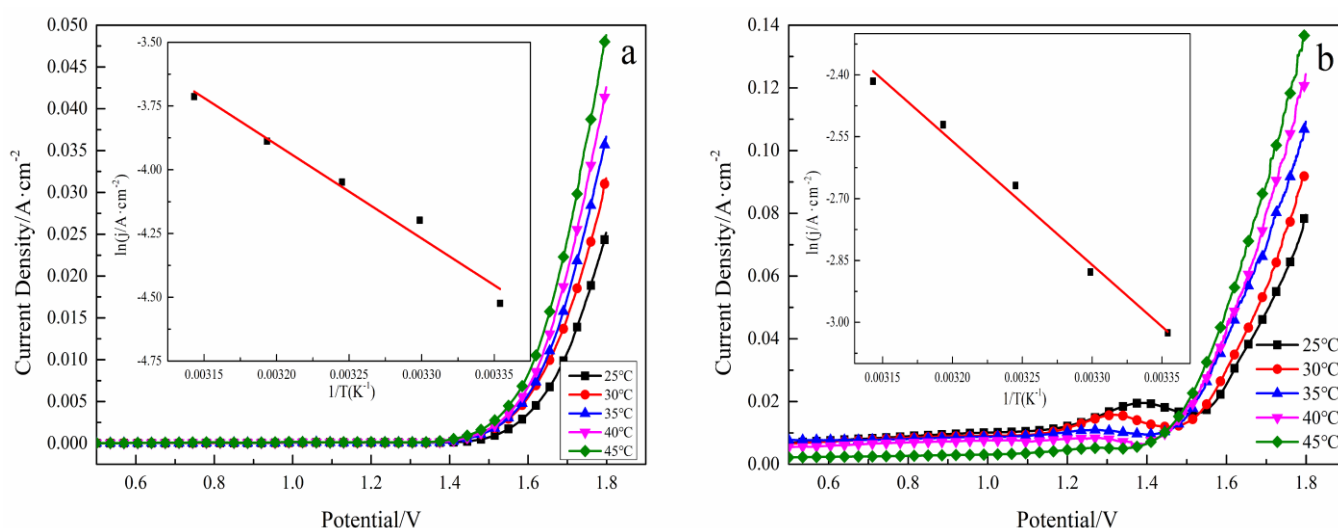


Figure 15. Linear sweep voltammograms and $\ln j-T^{-1}$ linear fitting curves of the flat-PbO₂ electrode(a)and 3D-PbO₂ electrode(b) at different temperatures in 0.5 mol·L⁻¹ Na₂SO₄ solutions at 25°C

Table 6. Oxygen evolution apparent activation energy of flat-PbO₂ electrode and 3D-PbO₂ electrode

Electrode	flat-PbO ₂ Electrode	3D-PbO ₂ Electrode
Ea/kJ·mol ⁻¹	30.53	24.92

3.4.6 Electrochemical impedance spectroscopy

EIS can be used to determine the catalytic oxygen evolution on the surface of different electrode materials, such as the adsorption and desorption of an electrolyte [37]. To study the chemical kinetics on the surface of an electrode, EIS is often used to study the gas evolution reaction on the surface of solid electrodes. Fig. 16 shows the Nyquist diagram and the equivalent circuit diagram of the flat-PbO₂ and 3D-PbO₂ electrodes in a 0.5 mol·L⁻¹ Na₂SO₄ solution. Table 7 shows the equivalent circuit

component parameters of the different electrodes. From the Nyquist diagram, it can be seen that both electrode materials had a capacitive arc resistance in the high-frequency region, which characterizes the electrochemical reaction process between the electrode oxidation layer and the solution interface. Charge transfer step was the main control step in the electrode reaction, the equivalent circuit can be represented by $LR_s(C_{dl}R_{ct})Z_w$, where the formation of an inductor L is due to the shielding effect caused by the close distance between the tip of the capillary and the electrode, R_s is the solution resistance, C_{dl} is the double-layer capacitance and R_{ct} is the charge transfer resistance in the electrochemical reaction process. The roughness of the 3D-PbO₂ electrode surface led to a variation in the double-layer capacitance and a non-uniform electric field, resulting in the dispersion effect, which is indicated by the irregular semicircle in the Nyquist plot. In the equivalent circuit, the constant phase angle element Q was used to replace the double-layer capacitance C_{dl} , and n is the corresponding dispersion coefficient. Both electrodes experienced Warburg impedance due to the diffusion barrier caused by the adsorption of oxygen.

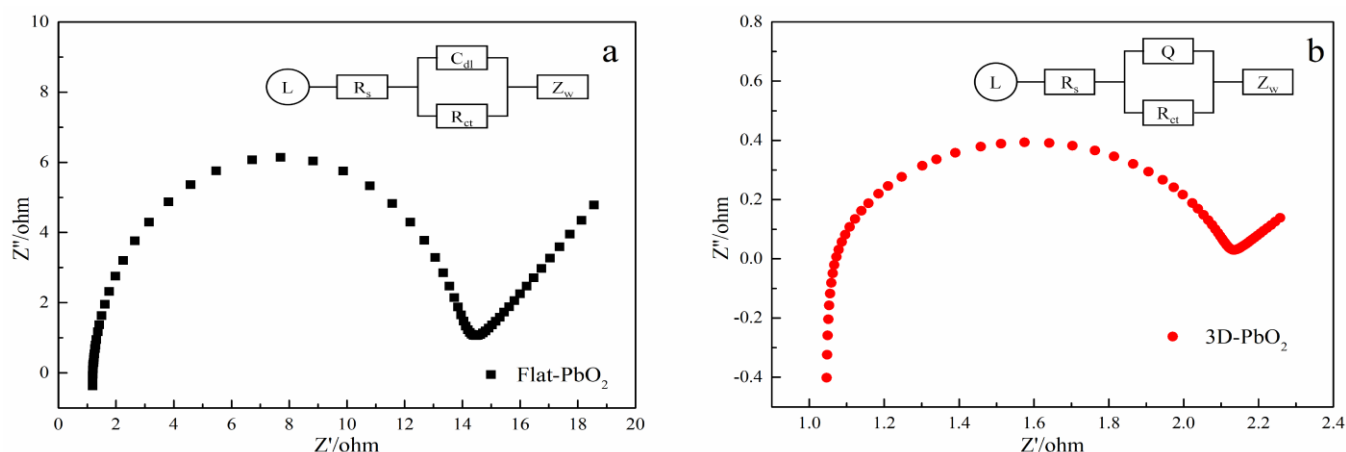


Figure 16. Nyquist diagrams and equivalent circuit of the flat-PbO₂ electrode (a) and 3D-PbO₂ electrode (b)

Table 7. Fitted EIS parameters of the flat-PbO₂ electrode and 3D-PbO₂ electrode

Electrode	L (H·cm ⁻²)	R (Ω·cm ²)	C _{dl} (F·cm ⁻²)	R _{ct} (Ω·cm ²)	Z _w (S·sec ^{0.5} ·cm ⁻²)	
flat-PbO ₂ Electrode	7.305×10 ⁻¹⁰	1.197	1.453×10 ⁻⁴	12.43	0.2631	
Electrode	L (H·cm ⁻²)	R (Ω·cm ²)	Q (S·s ⁻ⁿ ·cm ⁻²)	n	R _{ct} (Ω·cm ²)	Z _w (S·sec ^{0.5} ·cm ⁻²)
3D-PbO ₂ Electrode	8.153×10 ⁻⁷	1.039	1.114×10 ⁻³	0.8	1.081	9.51

The values of the fitting parameters obtained from the abovementioned equivalent circuit diagrams were all less than 10⁻³, which shows that the equivalent circuit diagrams reflected the oxygen evolution behavior of the electrode material in the 0.5 mol·L⁻¹ Na₂SO₄ solution. The 3D-PbO₂ electrode materials had an increased Warburg impedance due to a large number of oxygen atoms and oxygen

molecules adsorbed on the electrode surface during the catalytic process, which affected the diffusion of OH⁻ from the solution body to the electrode surface. The double-layer capacitance (C_{dl}) and R_{ct} can be used to characterize the electrocatalytic activity of electrode materials for oxygen evolution. Small R_{ct} values and large C_{dl} values are more favorable for the oxygen evolution reaction. Thus, the electrocatalytic activity of the electrode material can be explained. The R_{ct} and C_{dl} values of the 3D-PbO₂ were 1.081 $\Omega \cdot \text{cm}^2$ and $1.114 \times 10^{-3} \text{ S} \cdot \text{s}^{-n} \cdot \text{cm}^{-2}$, respectively, while the R_{ct} and C_{dl} values of the flat-PbO₂ were 12.43 $\Omega \cdot \text{cm}^2$ and $1.453 \times 10^{-4} \text{ F} \cdot \text{cm}^{-2}$, respectively. The larger C_{dl} value indicated that 3D-PbO₂ had a larger electrochemical active surface area, this is in agreement with the results of CV. Also, the 3D-PbO₂ electrode had a smaller R_{ct} , reduction of the charge transfer resistance proves that the porous structure promotes the electron transfer process and is conducive to the electrocatalytic reaction. Zhang et al.[38] prepared a porous PbO₂-ZrO₂ electrode by anodizing method. In 0.5 mol $\cdot \text{L}^{-1}$ Na₂SO₄ solution, the R_{ct} of the electrode is 30.59 $\Omega \text{ cm}^2$. In contrast, the R_{ct} of 3D-PbO₂ electrode in this study is only 1.081 $\Omega \text{ cm}^2$, which is much lower than the charge transfer resistance of porous PbO₂-ZrO₂, so it can carry out oxygen evolution reaction faster. Therefore, the 3D-PbO₂ anode material had better electrocatalytic activity during the catalytic oxygen evolution reaction.

4. CONCLUSION

During the preparation of the 3D-PbO₂ anode material, the current density determined whether the oxygen bubble can continuously escape, and the influence on the structure of the oxygen bubble was limited after a stable escape. The structure of the PbO₂ was influenced by the change in the Pb²⁺ concentration, and a suitable Pb ion concentration can allow the electrode surface to produce a uniform and ordered pore wall and pore channel structure, forming a complete three-dimensional porous structure. A plating solution with a suitable pH value can promote the enrichment and release of oxygen bubbles, producing a large number of small oxygen bubbles, and enriching the substrate surface to form a uniform template of oxygen bubbles.

The process conditions used to prepare 3D-PbO₂ anode materials by the oxygen bubble template method were studied. The optimum preparation conditions were as follows: current density of 2.0 A $\cdot \text{cm}^{-2}$, Pb²⁺ concentration of 0.4 mol $\cdot \text{L}^{-1}$ and electrolyte pH value of 3.0.

Compared with the flat-PbO₂ anode, the porous PbO₂ anode material had a higher exchange current density j^0 , lower E_a and lower R_{ct} . According to CV data, the 3D-PbO₂ anode material had a large q_T^* of $4.87 \times 10^{-2} \text{ C} \cdot \text{cm}^{-2}$, which is approximately ten times as large as that of the planar PbO₂ electrode. The three-dimensional porous structure increased the active surface area of the PbO₂ electrode, which led to additional active sites on the electrode surface and an improved electrocatalytic activity during the catalytic process.

ACKNOWLEDGMENTS

This work was financially supported by the National Natural Science Foundation of China (No. 51464021). We thank AJE (www.aje.com) for its linguistic assistance during the preparation of this manuscript.

References

1. R. Amadelli, A. Maldotti, A. Molinari, F.I. Danilov, A.B. Velichenko, *J. Electroanal. Chem.*, 534 (2002) 1.
2. M. Musiani, F. Furlanetto, R. Bertocello, *J. Electroanal. Chem.*, 465 (1999) 160.
3. S. Cattarin, I. Frateur, P. Guerriero, M. Musiani, *Electrochim. Acta*, 45 (2000) 2279.
4. Y. Li, L. Jiang, F. Liu, J. Li, Y. Liu, *RSC Advances*, 4 (2014) 24020.
5. Z. Wang, Y. Mao, M. Xu, Y. Wei, Y. Hu, C. Zhu, W. Fang, F. Wang, *J. Electrochem. Soc.*, 164 (2017) H981.
6. X. Chen, P. Kuang, C. Chen, X. Zhang, T. Huang, L. Zhang, A. Yu, *Int. J. Electrochem. Sci.*, 13 (2018) 3309.
7. L. Wu, J. Xia, H. Cao, Y. Tang, G. Hou, G. Zheng, *Int. J. Hydrogen. Energ.*, 42 (2017) 10813.
8. L. Wu, J. Xia, G. Hou, H. Cao, Y. Tang, G. Zheng, *Electrochim. Acta*, 191 (2016) 375.
9. Q. Shao, L. Wang, X. Wang, M. Yang, S. Ge, X. Yang, J. Wang, *Solid State Sci.*, 20 (2013) 29.
10. Y. Fu, Z. Jin, Z. Liu, Y. Liu, W. Li, *Mater. Lett.*, 62 (2008) 4286.
11. S. Chai, G. Zhao, Y. Wang, Y.n. Zhang, Y. Wang, Y. Jin, X. Huang, *Applied Catalysis B: Environmental*, 147 (2014) 275.
12. K.M. Chahrour, N.M. Ahmed, M.R. Hashim, N.G. Elfadill, M.A. Qaeed, M. Bououdina, *Superlattice. Microst.*, 76 (2014) 197.
13. B. Luo, X. Li, X. Li, W. Feng, *Asian. J. Chem.*, 25 (2013) 9927.
14. X. Hu, F. Cheng, X. Han, T. Zhang, J. Chen, *Small*, 11 (2014) 809.
15. B. Qi, H. Yang, K. Zhao, M.M. Bah, X. Bo, L. Guo, *J. Electroanal. Chem.*, 700 (2013) 24.
16. N. Comisso, S. Cattarin, P. Guerriero, L. Mattarozzi, M. Musiani, E. Verlato, *Electrochem. Commun.*, 73 (2016) 59.
17. Y. Yao, C. Huang, Y. Yang, M. Li, B. Ren, *Chem. Eng. J.*, 350 (2018) 960.
18. N. Comisso, M. Rancan, L. Armelao, S. Barison, S. Cattarin, P. Guerriero, L. Mattarozzi, M. Musiani, L. Vázquez-Gómez, E. Verlato, *Electrochim. Acta*, 341 (2020) 136056.
19. Y. Yao, X. Chen, N. Yu, H. Dong, H. Wang, *J. Electrochem. Soc.*, 164 (2017) E48.
20. A.J. Bard, L.R. Faulkner, *Dianhuaxue*, 7 (2001) 255.
21. Sengupta, Srijan, Patra, Arghya, Jena, Sambedan, Das, Karabi, Siddhartha, *Metall. Mater. Trans. A*, 49 (2018) 920.
22. Chen, Xin, Naichuan, Dong, Haishu, Wang, Haoren, Yao, Yingwu, *J. Electrochem. Soc.*, 164 (2017) E48.
23. R.D. Marco, A. Lowe, M. Sercombe, P. Singh, *Electrochim. Acta*, 51 (2006) 2088.
24. N. Comisso, S. Cattarin, P. Guerriero, L. Mattarozzi, M. Musiani, E. Verlato, *Electrochim. Acta*, 200 (2016) 259.
25. X. Li, G. Yang, S. Li, N. Xiao, N. Li, Y. Gao, D. Lv, L. Ge, *Chem. Eng. J.*, 379 (2020) 122350.
26. U. Holzwarth, N. Gibson, *Nature nanotechnology*, 6 (2011) 534
27. W. Wang, X. Duan, X. Sui, Q. Wang, L. Chang, *Electrochim. Acta*, 335 (2020) 135649.
28. T. Duan, Y. Chen, Q. Wen, Y. Duan, *RSC Adv.*, 4 (2014) 57463.
29. W. Zhao, J. Xing, D. Chen, Z. Bai, Y. Xia, *RSC Advances*, 5 (2015) 26530.
30. S.-B. Yoon, H.-K. Kim, K.C. Roh, K.-B. Kim, *J. Electrochem. Soc.*, 162 (2015) A667.
31. J. Zhu, Y. Xu, *Electrochim. Acta*, 265 (2018) 47.
32. F. Montilla, E. Morallón, A. De Battisti, J.L. Vázquez, *J. Phys. Chem. B*, 108 (2004) 5036.
33. Z. Xiezheng, L. Siqi, Y. Hongxia, X. Anlin, L. Jiansheng, S. Xiuyun, S. Jinyou, H. Weiqing, W. Lianjun, *J. Electroanal. Chem.*, 826 (2018) 181.
34. J.J. Zhang, J.M. Hu, J.Q. Zhang, C.N. Cao, *Int. J. Hydrogen. Energ.*, 36 (2011) 5218.
35. Q. Che, H. Yang, L. Lu, Y. Wang, *J. Mater. Sci.: Mater. Electron.*, 24 (2013) 524.
36. L. Gui, Z. Chen, Y. Song, W. Zhu, Q. Yu, D. Wu, T. Zheng, *J. Electrochem. Soc.*, 166 (2019) E384.
37. T. Chen, H. Huang, H. Ma, D. Kong, *Electrochim. Acta*, 88 (2013) 79.

38. L. Zhang, F. Wei, Q. Zhao, X. Chen, Y. Yao, *Res. Chem. Intermediat*, 46 (2019) 1389.

© 2021 The Authors. Published by ESG (www.electrochemsci.org). This article is an open access article distributed under the terms and conditions of the Creative Commons Attribution license (<http://creativecommons.org/licenses/by/4.0/>).